

Nonprecious-Metal-Assisted Photochemical Hydrogen Production from *ortho*-Phenylenediamine

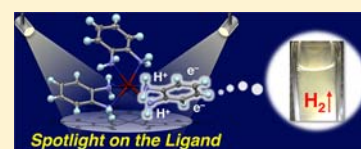
Takeshi Matsumoto,[‡] Ho-Chol Chang,^{*,†} Masanori Wakizaka,[†] Sho Ueno,[†] Atsushi Kobayashi,[†] Akira Nakayama,[†] Tetsuya Taketsugu,^{‡,†} and Masako Kato^{*,‡,†}

[†]Department of Chemistry, Faculty of Science, Hokkaido University, North-10, West-8, Kita-ku, Sapporo 060-0810, Japan

[‡]Center for Strategic Utilization of Elements, Faculty of Science, Hokkaido University, North-10, West-8, Kita-ku, Sapporo 060-0810, Japan

S Supporting Information

ABSTRACT: The combination of *o*-phenylenediamine (opda), which possesses two proton- and electron-pooling capability, with Fe(II) leads to the photochemical hydrogen-evolution reaction (HER) in THF at room temperature without addition of photosensitizers. From the THF solution, the tris(*o*-phenylenediamine) iron(II) complex, [Fe^{II}(opda)₃](ClO₄)₂ (1), was isolated as a photoactive species, while the deprotonated oxidized species was characterized by X-ray crystallographic analysis, electrospray ionization mass spectrometry, and UV–vis NIR spectra. Furthermore, the HER is photocatalyzed by hydroquinone, which serves as a H⁺/e⁻ donor. The present work demonstrates that the use of a metal-bound aromatic amine as a H⁺/e⁻ pooler opens an alternative strategy for designing nonprecious-metal-based molecular photochemical H₂ production/storage materials.



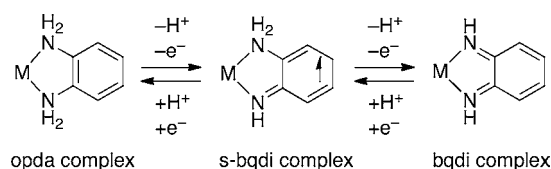
INTRODUCTION

Energy is the most important issue in the 21st century.¹ The growing global energy demand, decreasing fossil fuel supply, and increased concerns over climate issues have spurred the development of alternative and sustainable energy carriers.² Among the several types of energy carriers,³ molecular hydrogen is one of the most promising and cleanest energy carriers with the least effect on the environment.⁴ Therefore, the creation of hydrogen production/storage systems is currently the subject of intensive investigations.⁵ The development of materials for hydrogen production/storage has been investigated using a wide range of materials, such as metal,⁶ complex,⁷ and chemical hydrides,⁸ clathrates,⁹ inorganic¹⁰ and organic nanotubes,¹¹ and metal–organic frameworks.^{5a,12} In particular, organic hydrides are fascinating hydrogen production/storage materials that have excellent values for gravimetric capacities (e.g., 7.1 wt %, 64.8 kg/m³ for benzene/cyclohexane conversion).^{5b} Recently, quinoline/1,2,3,4-tetrahydroquinoline¹³ or secondary alcohol/ketone¹⁴ systems have been reported as efficient hydrogen production/storage material that can be operated at relatively low temperatures (~80–140 °C), especially in the hydrogen-evolution reaction (HER) processes, using Ir complexes as a catalyst. However, even in these excellent examples, the operating temperature for the HER is higher than those of hydrogenation-reaction processes. Therefore, the creation of a HER that can be driven at moderate temperature¹⁵ with the use of nonprecious-metal catalysts¹⁶ is an important issue to be investigated.

These considerations inspired us to utilize an organic skeleton possessing multiproton- and electron-pooling capability. The aromatic amines or hydroxides, such as phenylenediamine¹⁷ or hydroquinone¹⁸ derivatives, are widely known to possess 2H⁺/2e⁻ pooling capability. Furthermore, *o*-

phenylenediamine (opda) has a coordinating ability toward transition-metal ions and undergoes multiproton- and electron-transfer processes to produce the corresponding oxidized species, such as semibenzoquinodiiimine (s-bqdi) or *o*-benzoquinodiiimine (bqdi) complexes.¹⁹ Therefore, they should be fascinating candidates as building modules for multiproton- and electron-pooling materials (Chart 1).

Chart 1. H⁺ and e⁻ Pooling Activity of Opda Complexes



The ultrafast dynamics of N–H σ -bond activation pathways were previously investigated for aromatic amines, such as aniline, using several spectroscopic and theoretical techniques.²⁰ In these reactions, it was elucidated that the generation of transient anilino radical species (C₆H₅NH \cdot) via hydrogen atom elimination was initiated by photoexcitation of $\pi\pi^*$ transition through 3s Rydberg states of the nitrogen atoms. Similar photoreactions were also investigated for aromatic diamines, such as opda and *p*-phenylenediamine.²¹ In these cases, transient bqdi and *p*-benzoquinodiiimine intermediates were detected by infrared spectra, as the results of photochemical N–H σ -bond activations and hydrogen atom eliminations. These studies prompted us to investigate the

Received: March 11, 2013

Published: April 1, 2013

photoreaction of opda interacting with nonprecious-metal ions, where the photoreactivity of opda was expected to be influenced by the metal ions. In this report, we describe the structure, multiple H^+/e^- transfer reactions, and photochemical HER utilizing **1**, $[Fe^{II}(opda)_3](ClO_4)_2$, which can be isolated by a one-pot reaction between 3 equiv of opda and $Fe(II)$ ion.

EXPERIMENTAL SECTION

General Procedures. All synthetic operations and measurements were performed under a N_2 atmosphere using Schlenk-line techniques. $[Fe^{II}(H_2O)_6](ClO_4)_2$ was purchased from Aldrich. *o*-Phenylenediamine and hydroquinone (HQ) were purchased from Wako Pure Chemical Industries and used as received. Deuterated opda ($C_6H_4N_2D_4$) and HQ ($C_6H_4O_2D_2$) were prepared according to conventional methods (see Supporting Information). *n*-Hexane and tetrahydrofuran (THF) were purchased from Kanto Chemical Co. Inc. and distilled twice from Na metal under a N_2 atmosphere. Dichloromethane (CH_2Cl_2), *tert*-butyl alcohol (*t*-BuOH), methanol (MeOH), and toluene were purchased from Wako Pure Chemical Industries and used without purification. All of the solvents were finally degassed in at least four freeze–pump–thaw cycles just prior to use. Molecular sieves (4 Å, MS4A) were purchased from Wako Pure Chemical Industries and activated by heating in vacuo prior to use. Caution! Although we experienced no difficulties with the perchlorate salts, they should be regarded as potentially explosive and therefore handled with care.

Synthesis of $[Fe^{II}(opda)_3](ClO_4)_2 \cdot THF$ (1·THF). *n*-Hexane/THF mixed solvent (v:v = 2:1) (20 mL) was layered onto a colorless THF solution (10 mL) of $[Fe^{II}(H_2O)_6](ClO_4)_2$ (1.09 g, 3 mmol). Then, colorless *n*-hexane/THF (v:v = 1:1) solution (30 mL) of opda (975 mg, 9 mmol) was layered on this solution. Storage of the mixture for 4 d at room temperature afforded crystals suitable for X-ray crystallographic analysis. After filtration and washing with THF (2 mL \times 2), drying in vacuo, afforded 1·THF as colorless crystals in 36% yield. Anal. found: C, 40.49; H, 4.91; N, 12.77. Calcd. for $C_{22}H_{32}Cl_2FeN_6O_9$ (1·THF): C, 40.57; H, 4.94; N, 12.90. $\chi_M T_{300K} = 3.96$ emu·K·mol⁻¹.

Synthesis of $[Fe^{II}(bqdi)_3](ClO_4)_2 \cdot THF$ (2·THF).^{19b} The complex 1·THF (912 mg, 1.4 mmol) was dissolved in CH_2Cl_2/t -BuOH mixed solvent (v:v = 1:1) (50 mL) to afford a white suspension, with the copresence of MS4A (20 g). O_2 gas was slowly introduced to this suspension, and the color of the suspension changed to navy after 5 min and to dark navy after 1 h. After bubbling O_2 for 5 h, the color of the suspension was finally bright green. The MS4A was removed by filtration, and the green product was extracted using MeOH (40 mL \times 2). After evaporation of the solvent, a dark-green powder was obtained and washed with THF (15 mL) and toluene (10 mL \times 2). Drying in vacuo afforded **2** as a greenish purple powder in 38% yield. ¹H NMR (270 MHz, CD_3CN , 298 K) δ 6.95–6.99 (m, 6H), 7.06–7.10 (m, 6H), 11.75 (br s, 6H). Diamagnetic. Anal. found: C, 39.76; H, 4.02; N, 12.49. Calcd. for $C_{22}H_{28}Cl_2FeN_6O_{10}$ (2·THF + H_2O): C, 39.84; H, 4.26; N, 12.67. For synthesis of a crystalline sample suitable for X-ray crystallographic analysis, this powder sample (5 mg) was dissolved in THF (2.5 mL), then *n*-hexane (2.5 mL) was layered onto this solution. After storage of this solution for 5 d at room temperature, greenish purple crystals of 2·THF were obtained.

Equipment Used in Photochemical HERs. A 100 W xenon lamp (LAX-103, Asahi Spectra Co., Ltd.) was used as the light source with quartz light guide ($\Phi 5 \times 1000L$ UD0030). For photochemical HER under irradiation or in the dark, 500 W xenon lamp (SX-UI500XQ, Ushio Inc.) with a quartz light guide (GFQ5L1000) was used as the light source. The light intensity was measured using a power meter (NOVA, Ophir Optronics Ltd.) and a thermopile sensor (3A, Ophir Optronics Ltd.). The amount of photochemically evolved H_2 was determined using a gas chromatograph (GC) (Shimadzu GC-14B, Ar carrier) equipped with a ShinCarbon ST 2 m long packed column (Shinwa Chemical Industries Ltd.) and a recorder (Shimadzu C-R8A Chromatopac Data Processor). For $H_2/HD/D_2$ detections, the gas samples were analyzed using a GC (Shimadzu GC-2014ATF+GC Solution, He carrier) equipped with 8% (w/w) KOH coated on an

activated alumina column, that was immersed in liquid N_2 during the GC measurements, and thermal conductivity detector.

Photochemical HERs. For photochemical hydrogen evolution, each sample was prepared in a handmade Schlenk flask-equipped quartz cell 182 mL in volume. For HER from opda without Fe^{II} ion, opda (25.9 mg, 2.39×10^{-4} mol) was dissolved in 4 mL of THF in the presence of ground MS4A (250 mg) under a N_2 atmosphere. On the other hand, for the reaction from opda in the presence of Fe^{II} ion, THF (4 mL) solution of $[Fe^{II}(H_2O)_6](ClO_4)_2$ (28.9 mg, 7.98×10^{-5} mol) was introduced to the opda (25.9 mg, 2.39×10^{-4} mol) in the presence of ground MS4A (250 mg) under a N_2 atmosphere. Each sample flask was doubly sealed with rubber septa. Before irradiation, gas (0.3 mL) was collected from the headspace using a gastight syringe (Tokyo Garasu Kikai Co. Ltd.) and analyzed by GC to confirm the successful N_2 purge. Then, the samples were irradiated using the 100 W xenon lamp in a water bath at room temperature. The gas samples (0.3 mL) were collected from the headspace at each analysis time for determination of the amount of H_2 evolved as a function of the irradiation time.

Photochemical HER with HQ. For photochemical H_2 evolution from 3opda/ $[Fe^{II}(H_2O)_6](ClO_4)_2/10HQ/THF$ suspension, the same reaction systems as the aforementioned cases were used, but the sample preparation procedures were different from those cases. The THF (2 mL) solution of $[Fe^{II}(H_2O)_6](ClO_4)_2$ (28.9 mg, 7.98×10^{-5} mol) was added to the opda (25.9 mg, 2.39×10^{-4} mol) in the presence of ground MS4A (250 mg) under a N_2 atmosphere and stirred for 30 s at room temperature. A THF solution (2 mL) of HQ (87.9 mg, 7.98×10^{-4} mol) was added to this white suspension. In these cases, no special changes were noticed in the appearance of the suspension. After the sample preparation, photochemical HERs were investigated by similar methods to those mentioned above.

Photochemical HER Using Opda in THF- d_8 . For photochemical HER, the sample was prepared in a quartz cell equipped with a three-way cock and aluminum gas sampling bag (GL Sciences Inc., AAK-1L) in which the quartz cell head is ~ 10 mL in volume. $[Fe^{II}(H_2O)_6](ClO_4)_2$ (21.7 mg, 5.99×10^{-5} mol) was dissolved in the degassed THF- d_8 (3 mL), and this solution was introduced to the opda (19.4 mg, 1.79×10^{-4} mol) in the presence of MS4A (190 mg) under a N_2 atmosphere. Before irradiation, the three-way cock and stopcock of the gas sampling bag were opened to connect the sample and aluminum gas bag to introduce the evolved H_2 into the bag. Then, the samples were irradiated in a water bath at room temperature. After the irradiation for 50 h, three-way cock and stopcock of gas sampling bag were closed, and gas sample in the bag was analyzed.

Photochemical HER Using Opda- d_4 in THF. The general operating procedures were the same as with those for HER using THF- d_8 , except for using $[Fe^{II}(H_2O)_6](ClO_4)_2$ (28.9 mg, 7.98×10^{-5} mol), opda- d_4 (25.9 mg, 2.39×10^{-4} mol), and THF (4 mL) in the presence of MS4A (250 mg).

Photochemical HER Using HQ- d_2 . $[Fe^{II}(H_2O)_6](ClO_4)_2$ (28.9 mg, 7.98×10^{-5} mol) was dissolved in degassed THF (2 mL), and this solution was added to the opda (25.9 mg, 2.39×10^{-4} mol) in the presence of MS4A (250 mg) under a N_2 atmosphere. Then, a THF (2 mL) solution of HQ- d_2 (89.4 mg, 7.98×10^{-4} mol) was added to this suspension. The photochemical reaction and evolved gas analysis were carried out using similar procedures to those used for $[Fe^{II}(H_2O)_6](ClO_4)_2$ and opda in THF- d_8 , except for the irradiation time (200 h).

Computational Details. Geometry optimization for $[Fe^{II}(opda)_3]^{2+}$, opda, and $[Fe^{II}(bqdi)_3]^{2+}$ in the electronic ground state was carried out in THF employing density functional theory (DFT) with the B3LYP combination of exchange and correlation functionals. The initial structures of $[Fe^{II}(opda)_3]^{2+}$ and $[Fe^{II}(bqdi)_3]^{2+}$ were taken from the X-ray crystallographic data. No symmetry constraints were imposed for $[Fe^{II}(opda)_3]^{2+}$ and opda, while C_3 symmetry was used for $[Fe^{II}(bqdi)_3]^{2+}$. The spin multiplicities were set to quintet for $[Fe^{II}(opda)_3]^{2+}$ and singlet for $[Fe^{II}(bqdi)_3]^{2+}$ and opda. The solvent effects were taken into account by the polarizable continuum solvation model (PCM),²² and the radii were taken from the UFF force field.²³ The SDD effective core potential (ECP) and associated basis set were used for the Fe atom,

and a 6-31G(d) basis set was employed for all other atoms. After the geometry optimization, the time-dependent (TD) DFT calculations²⁴ were performed to evaluate the vertical excitation energies at the equilibrium structures in THF employing the BLYP functionals with the long-range correction (LC)²⁵ (LC-BLYP). The basis set for C and N atoms was replaced by 6-31+G(d) in TD-DFT calculations to account for the Rydberg states in opda. All calculations were performed using the Gaussian 09 package.²⁶

The optimized structures and the Cartesian coordinates are given in Supporting Information. It is found that the optimized structures for $[\text{Fe}^{\text{II}}(\text{opda})_3]^{2+}$ and $[\text{Fe}^{\text{II}}(\text{bqdi})_3]^{2+}$ are very close to those of the X-ray crystallographic data.

In the TD-DFT calculations of opda, the first (S_1) and third (S_3) singlet excitations are characterized by $^1\pi\pi^*$ transitions, while the second (S_2) singlet excited state exhibits $^1\pi\sigma^*$ character. The transitions to $S_1(^1\pi\pi^*)$ and $S_3(^2^1\pi\pi^*)$ are mainly viewed as $2\pi \rightarrow 1\pi^*$ and $2\pi \rightarrow 2\pi^*$ excitations, respectively (see Figure S6 for relevant orbitals). The S_2 state involves an excitation of $2\pi \rightarrow 1\sigma^*$ and exhibits a 3s Rydberg character associated with the N atoms. This $^1\pi\sigma^*$ state is a dark state, and therefore it was not detected in the experimental spectra. The vertical excitation energies for $^1\pi\pi^*$ and $^2^1\pi\pi^*$ are calculated to be 4.97 eV (252 nm) and 5.59 eV (222 nm), respectively, and these values are overestimated in comparison to the experimental values (see Supporting Information). In general, the LC correction has a tendency to yield higher excitation energy than that without the LC correction even in the valence excitations. In fact, excitation energies calculated without the LC correction (BLYP functional) are 4.22 eV (294 nm) and 4.90 eV (253 nm) for $^1\pi\pi^*$ and $^2^1\pi\pi^*$, respectively, and these values are in good agreement with the experimental values. However, as is shown below in the calculations on $[\text{Fe}^{\text{II}}(\text{opda})_3]^{2+}$, the charge-transfer states that involve the ligand–metal charge transfer (LMCT) are observed in the UV region, and hence the LC correction is essential to describe correctly the order of the excitations.

The calculated UV absorption spectra of $[\text{Fe}^{\text{II}}(\text{opda})_3]^{2+}$ are shown in Supporting Information, together with detailed information on selected excitations (Figure 4, see Supporting Information for the detailed information on selected excitations). The natural transition orbital (NTO) analysis²⁷ was carried out to understand better the results of the TD-DFT calculations. From this analysis, it is found that the first two low-lying peaks around 226 and 203 nm correspond to the $^1\pi\pi^*$ and $^2^1\pi\pi^*$ excitations of the opda ligand moiety, respectively, and the next peaks above 190 nm correspond to the LMCT transitions. The dominant NTO pairs for the representative transitions are shown in Figure 4c. Small blue-shifts of ~ 20 nm are observed for ligand $^1\pi\pi^*$ excitations when the $[\text{Fe}^{\text{II}}(\text{opda})_3]^{2+}$ complex is formed, but it is clear that the LMCT transition is well above the ligand $^1\pi\pi^*$ excitations. On the other hand, from the analysis for $[\text{Fe}^{\text{II}}(\text{bqdi})_3]^{2+}$, LMCT transitions are found in the longer wavelength regions that are not obtained for opda and $[\text{Fe}^{\text{II}}(\text{opda})_3]^{2+}$ (see Supporting Information). These results reflect the higher electron-accepting nature of the bqdi moieties in $[\text{Fe}^{\text{II}}(\text{bqdi})_3]^{2+}$, compared with those of $[\text{Fe}^{\text{II}}(\text{opda})_3]^{2+}$.

Physical Measurements. Elemental analyses were performed at the analysis center at Hokkaido University. UV–vis NIR spectra in solution were recorded on a Hitachi U-4100 spectrophotometer over the range 200–3300 nm at 296 K using crystalline samples of 1·THF and 2·THF. Infrared spectra were recorded on a Nicolet 6700 FT-IR spectrometer equipped with a Smart-Orbit (Diamond) ATR accessory. Magnetic susceptibility of the crystalline samples was measured using a Quantum Design MPMS-XL SQUID magnetometer with a magnetic field of 1 T. Diamagnetic corrections were made based on Pascal's constants.²⁸ ^1H NMR (270 MHz) spectra were measured in CD_3CN , CDCl_3 , THF- d_6 , or DMSO- d_6 with a JEOL EX-270 spectrometer. The signals from the residual solvent protons of CD_3CN (1.94 ppm), CDCl_3 (7.26 ppm), THF- d_6 (3.58 ppm), and DMSO- d_6 (2.50 ppm) were used as internal standards.²⁹

Crystallographic Data Collection and Refinement of Structures. Crystallographic measurements were performed on a Rigaku AFC-7R diffractometer equipped with a Mercury CCD area detector, and graphite-monochromated Mo $K\alpha$ radiation ($\lambda = 0.71069$

Å). Specimens of suitable size and quality were selected under paraffin oil and mounted on MicroMounts (MiTeGen). The crystal was cooled using a N_2 -flow-type temperature controller. The structures were solved by direct methods (SIR2004),³⁰ which successfully located nonhydrogen atoms. All calculations were performed using the CrystalStructure crystallographic software package,³¹ except for refinement calculations, which were performed using SHELXL-97.³² A summary of the crystallographic data for 1·THF and 2·THF is given in Table 1. Full crystallographic details have been deposited with the Cambridge Crystallographic Data Centre as supplementary publication no. CCDC-909643 for 1·THF and -909646 for 2·THF.

Table 1. Crystallographic Data for 1·THF and 2·THF

	1·THF	2·THF
formula	$\text{C}_{22}\text{H}_{32}\text{Cl}_2\text{FeN}_6\text{O}_9$	$\text{C}_{22}\text{H}_{26}\text{Cl}_2\text{FeN}_6\text{O}_9$
fw	651.28	645.24
crystal size (mm^3)	$0.30 \times 0.16 \times 0.16$	$0.40 \times 0.16 \times 0.08$
crystal system	monoclinic	monoclinic
space group	$P2_1/n$ (no. 14)	$P2_1/c$ (no. 14)
<i>a</i> (Å)	17.849(2)	14.7311(19)
<i>b</i> (Å)	8.3097(9)	9.9389(11)
<i>c</i> (Å)	18.998(2)	18.389(2)
β (°)	100.5257(15)	98.0500(18)
<i>V</i> (Å ³)	2770.4(6)	2665.8(6)
<i>T</i> (K)	150	150
<i>Z</i>	4	4
<i>D</i> _{calc} (g cm^{-3})	1.561	1.608
<i>F</i> (000)	1352	1328
μ (Mo $K\alpha$) (cm^{-1})	7.974	8.281
measured reflections	22454	21537
unique reflections	6242	6039
refined parameters	362	380
GOF on F^2	1.125	1.126
R_{int}	0.048	0.033
R_1^a	0.0566	0.0652
wR_2^b (all data)	0.1533	0.1761

$^a R_1 = \frac{\sum \|F_o\| - |F_c|}{\sum \|F_o\|}$. $^b wR_2 = \left\{ \frac{\sum w(F_o^2 - F_c^2)^2}{\sum w(F_o^2)^2} \right\}^{1/2}$.

RESULTS AND DISCUSSION

Photochemical HER from the Mixture of 3opda and Fe(II). The treatment of opda (2.39×10^{-4} mol) with $[\text{Fe}^{\text{II}}(\text{H}_2\text{O})_6](\text{ClO}_4)_2$ (7.98×10^{-5} mol) in THF immediately afforded a white suspension. On irradiation of the suspension with white light, gas evolution started, and GC analysis proved the formation of H_2 (Figure 1a, red circles, and see Supporting Information). After irradiation for 57 h, the white suspension had changed to a green suspension and the amount of H_2 reached almost a plateau value, 8.77×10^{-5} mol of H_2 , which leads to mole ratios of $[\text{evolved H}_2]/[\text{opda}] = 0.37$ and $[\text{evolved H}_2]/[\text{Fe}^{\text{II}}] = 1.10$. In contrast, the HER was not observed under a dark condition at all, suggesting HER was driven as a photochemical reaction (Figure 1b). Two further control experiments without either Fe(II) or opda under the same conditions showed that the evolved H_2 was only one-twelfth as much as that in the presence of Fe(II) or undetectable, respectively (Figure 1a, blue and black circles). These results clearly demonstrate that coexistence of opda and Fe(II) is necessary for efficient HER and stimulated us to characterize the active species of the HER.

Characterization of the Active Species of the HER. Slow diffusion of *n*-hexane/THF (*v*:*v* = 1:1) solution of 3 equiv

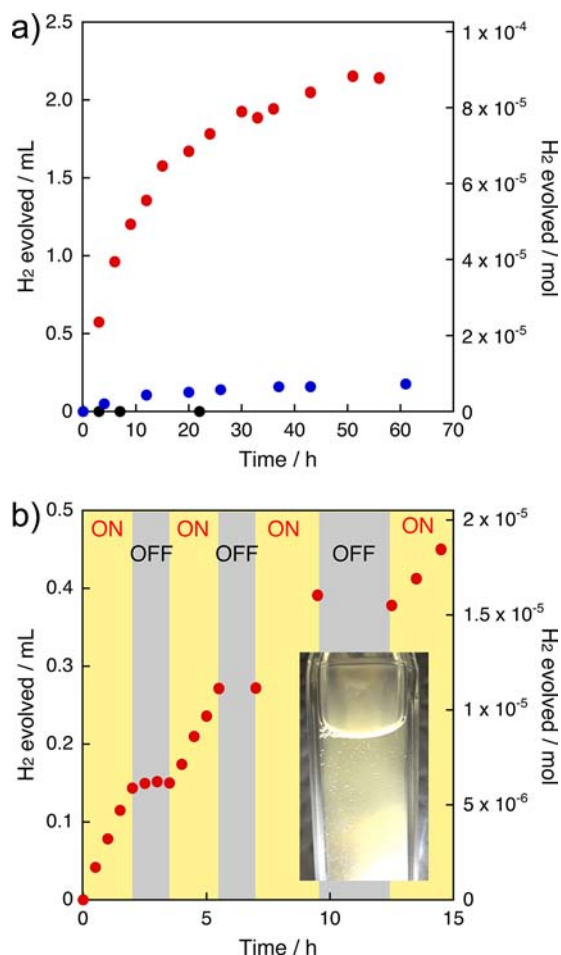


Figure 1. (a) Amounts of photochemically evolved H_2 from 3opda/ $[\text{Fe}^{\text{II}}(\text{H}_2\text{O})_6](\text{ClO}_4)_2/\text{THF}$ suspension (red circles), 3opda/THF solution (blue circles), and $[\text{Fe}^{\text{II}}(\text{H}_2\text{O})_6](\text{ClO}_4)_2/\text{THF}$ solution (black circles). (b) Photochemical HER from a 3opda/ $[\text{Fe}^{\text{II}}(\text{H}_2\text{O})_6](\text{ClO}_4)_2/\text{THF}$ suspension under irradiation or in the dark. The sample suspension was kept under irradiation by white light for 0–2.0, 3.5–5.5, and 7.0–9.5 h (yellow background) and kept in the dark for 2.0–3.5, 5.5–7.0, and 9.5–12.5 h (gray background). After 12.5 h, the sample was put under irradiation. Insert: photograph of photochemical HER. Bubbles were generated from the light path.

opda into a THF solution of $[\text{Fe}^{\text{II}}(\text{H}_2\text{O})_6](\text{ClO}_4)_2$ afforded air-sensitive colorless single crystals suitable for X-ray crystal structural analysis. The crystal is composed of a $[\text{Fe}(\text{C}_6\text{H}_4\text{N}_2\text{H}_4)_3]^{2+}$ cation and two ClO_4^- anions together with one THF molecule (see Supporting Information). The structure of the cation depicted in Figure 2 shows that three ligands (L1–L3) commonly coordinate to the Fe atom in bidentate chelating modes (see Supporting Information). The N–C (1.440(3)–1.450(3) Å) and the C–C bond distances of the six-membered ring are similar to those of non coordinating opda.³³ Here, we note that the dihedral angles (η) between the N–Fe–N and N–C–C–N planes indicate that the ligands are the neutral opda form with two protons on each sp^3 -type N atom. In addition, the Fe–N (2.204(2)–2.269(2) Å) bond distances and magnetic moment, $\chi_M T_{300\text{K}} = 3.96 \text{ emu}\cdot\text{K}\cdot\text{mol}^{-1}$, support the presence of a high-spin Fe(II) center.

All of these facts finally lead to the formulation of the crystal as $[\text{Fe}^{\text{II}}(\text{opda})_3](\text{ClO}_4)_2\cdot\text{THF}$ (1·THF), in which the ligands exist in the fully reduced form without forming oxidized s-bqdi or bqdi forms. Identical IR spectra were obtained for the crystal

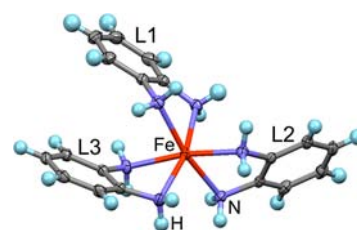


Figure 2. Molecular structure of the cation in 1·THF with thermal ellipsoid plots for Fe (brown), N (blue), and C (gray) (50% probability). Hydrogen atoms are depicted as ball-and-stick models colored light blue. THF and ClO_4^- are omitted for clarity (see Supporting Information for overall structure).

and the white powder prepared *in situ* before HER, indicating that both are 1·THF (see Supporting Information).

Source and Irradiation Light Dependence of the HER.

To obtain clear information on the H^+ source in the photochemical HER system, photoirradiation of the mixture of opda and $[\text{Fe}^{\text{II}}(\text{H}_2\text{O})_6](\text{ClO}_4)_2$ in THF- d_8 was carried out. The GC analyses revealed that only H_2 was obtained as the gaseous products, clearly excluding the contribution of the THF molecule as the H^+ source in this HER (Figure 3c). In

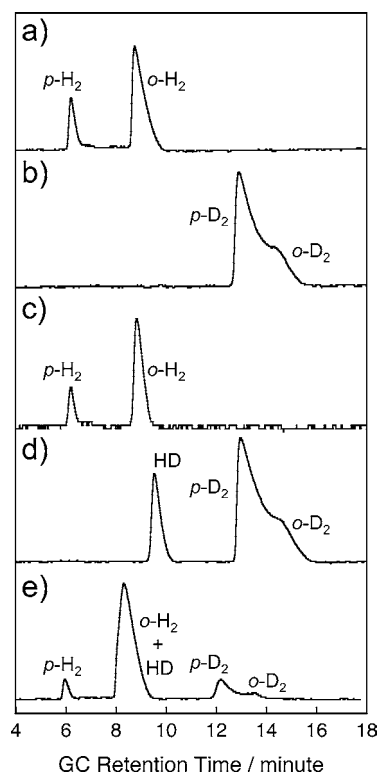


Figure 3. GCs of (a) H_2 and (b) D_2 standard gases, and photochemically evolved gas samples from (c) 3opda/ $[\text{Fe}^{\text{II}}(\text{H}_2\text{O})_6](\text{ClO}_4)_2/\text{THF}-d_8$, (d) 3opda- d_4 / $[\text{Fe}^{\text{II}}(\text{H}_2\text{O})_6](\text{ClO}_4)_2/\text{THF}$, and (e) 3opda/ $[\text{Fe}^{\text{II}}(\text{H}_2\text{O})_6](\text{ClO}_4)_2/10\text{HQ}-d_2/\text{THF}$ mixtures.

addition, the photoirradiation experiment using opda- d_4 ($\text{C}_6\text{H}_4\text{N}_2\text{D}_4$), in which the deuteration ratio on the amino moieties was determined to be 92% (see Supporting Information), and $[\text{Fe}^{\text{II}}(\text{H}_2\text{O})_6](\text{ClO}_4)_2$ in THF showed D_2 and HD evolution, showing that the H^+ in the photochemically evolved H_2 came from the amino protons of the opda moieties (Figure 3d).

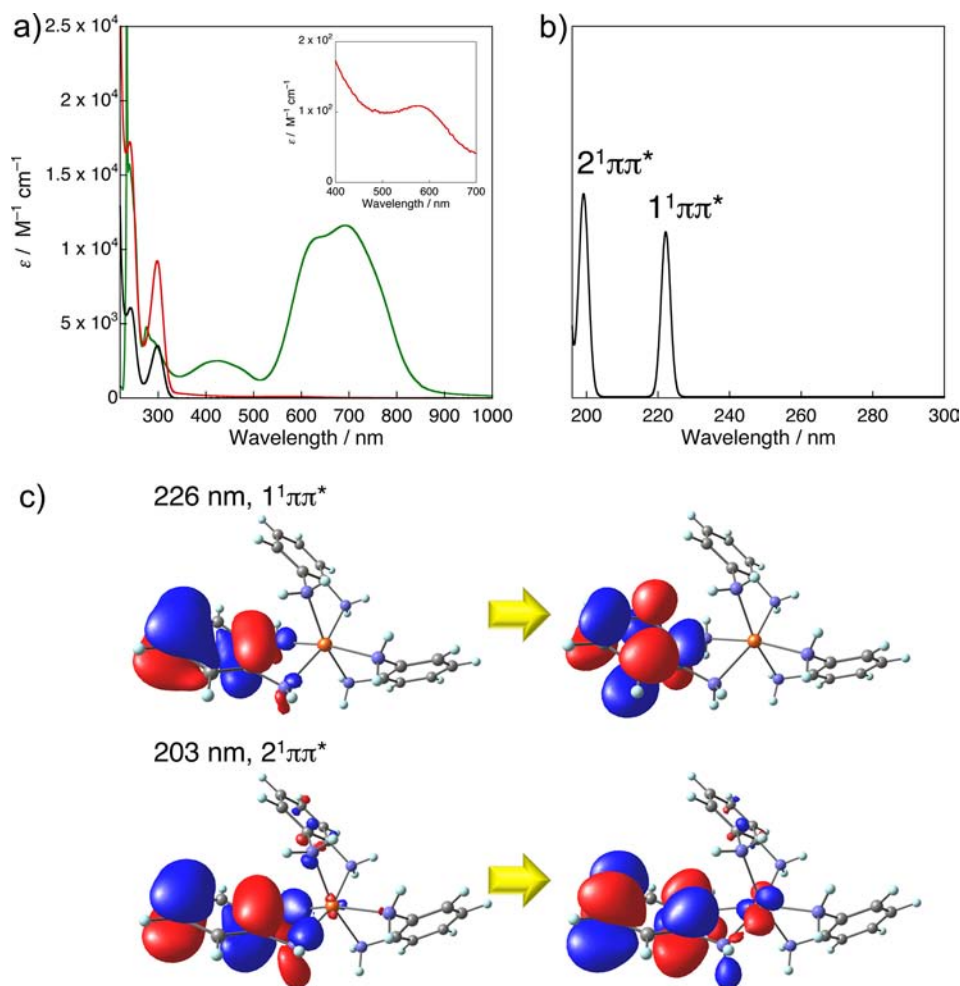


Figure 4. (a) UV-vis NIR spectra of **1** (red line) and opda (black line) in THF at 1×10^{-4} M. (b) Simulated absorption spectrum of $[\text{Fe}^{\text{II}}(\text{opda})_3]^{2+}$ in THF obtained by TD-DFT (LC-BLYP). (c) Dominant NTO pairs for selected ligand- $\pi\pi^*$ transitions of $[\text{Fe}^{\text{II}}(\text{opda})_3]^{2+}$ in THF. For each state, the “hole” is on the left, the “particle” on the right.

A UV-vis spectrum of **1** dissolved in THF is shown in Figure 4a (red line) together with that of opda (black line) at the same conditions, and the data are summarized in Supporting Information. The UV-vis spectrum of **1** shows two strong absorption bands in the UV region at 240 ($17\,230$) and 298 nm ($9230\text{ M}^{-1}\text{ cm}^{-1}$), which are similar in wavelength to those of opda observed at 242 (6080) and 298 nm ($3530\text{ M}^{-1}\text{ cm}^{-1}$). Complex **1** additionally shows a weak absorption band at 572 nm ($110\text{ M}^{-1}\text{ cm}^{-1}$), which could be assignable to an Fe(II)-centered d-d transition. To characterize these absorptions, the DFT calculations were performed for $[\text{Fe}^{\text{II}}(\text{opda})_3]^{2+}$ and opda with the solvents effects taken into account by the polarizable continuum solvation model. First, it was confirmed that the optimized geometry for $[\text{Fe}^{\text{II}}(\text{opda})_3]^{2+}$ in the electronic ground state was in good agreement with that obtained in the X-ray crystallographic analysis (see Supporting Information). The TD-DFT calculation suggested that the absorptions in the UV region were attributed to two $\pi\pi^*$ transitions ($1^1\pi\pi^*$ and $2^1\pi\pi^*$) localized on the opda moieties (see Figure 4b,c and Computational Details).

To ascertain the excitation that initiates the photochemical HER, excitation-light dependence was examined (see Supporting Information). By irradiation with visible light to the suspension for 19 h, no H_2 was obtained, suggesting that the excitation at 572 nm is negligible for the HER. On the other

hand, after irradiation with UV light at around 298 nm for 17 h, evolution of H_2 ($2.72\ \mu\text{mol}$) was obtained. These results indicate that the photochemical HER should be initiated by the $\pi\pi^*$ transition of the coordinating opda moiety. The apparent quantum yield (Φ) of this photochemical HER in the aforementioned conditions was estimated to be 3.39% (see Supporting Information for details of the calculation).³⁴

H⁺/e⁻ Pooling Ability of Opda. In the present photochemical HER, the role of the opda moiety as the H⁺ source for photochemical HER was successfully evaluated. These results inspired us to identify an electron source in the reaction. We found that complex **1** showed remarkable reactivity not only for photochemical reaction but also for air oxidation to produce a greenish-blue species both in $\text{CH}_2\text{Cl}_2/t\text{-BuOH}$ (v:v = 1:1)^{19a} and in THF solution under dark conditions. During this air oxidation, no HER was observed.

The single crystal of the oxidized species grown from hexane/THF mixed solvent revealed that the crystal was composed of a $[\text{Fe}(\text{C}_6\text{H}_4\text{N}_2\text{H}_2)_3]^{2+}$ cation and two ClO_4^- anions together with one THF molecule (Figure 5). The cationic moiety demonstrates significant shortening in the N-C ($1.301(3)$ – $1.319(3)$ Å) and Fe–N ($1.919(2)$ – $1.931(2)$ Å) bond distances compared with those of **1**·THF (see Supporting Information). In addition, the coplanarity of the N–Fe–N and N–C–C–N planes, together with the cyclohexa-3,5-diene

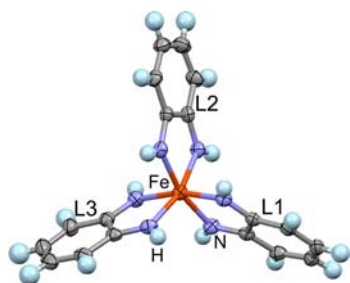


Figure 5. Molecular structure of the cation in 2·THF with thermal ellipsoid plots for Fe (brown), N (blue), and C (gray) (50% probability). Hydrogen atoms are depicted as ball-and-stick models colored light blue. THF and ClO_4^- are omitted for clarity.

character of the six-membered ring in each ligand indicate the sp^2 -type hybridization state of the coordinating N atoms, accompanying the imino-proton on each N atoms.^{19b–e,35} In contrast to the paramagnetic nature of 1·THF, the oxidized species shows diamagnetic character, indicative of a low-spin Fe(II) center because of the relatively stronger ligand field of the bqdi moiety compared with that of opda (see Supporting Information). Based on all of these structural features, the oxidized species can be finally assigned as $[\text{Fe}^{\text{II}}(\text{bqdi})_3]-(\text{ClO}_4)_2 \cdot \text{THF}$ (2·THF).^{19b}

In contrast to the case of 1, complex 2 shows characteristic absorption bands in the visible region at 420, 623, 692, and 770 nm, which were assigned as MLCTs and d–d transitions based on the TD-DFT calculations on the $[\text{Fe}^{\text{II}}(\text{bqdi})_3]^{2+}$ moiety (Figure 6, green solid line, and see Supporting Information).

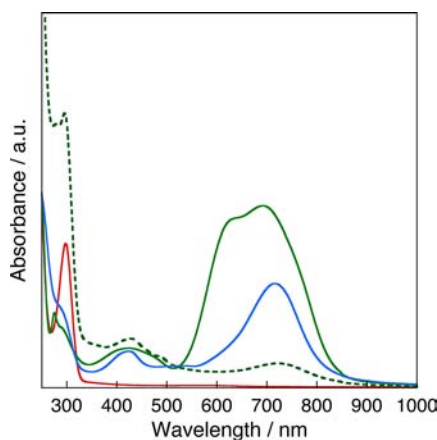


Figure 6. UV–vis NIR spectra of 1 (red solid line) and 2 (green solid line) (1×10^{-4} M), HER mixture from 3opda/ Fe^{II} /THF extracted by THF (green dashed line), and air-oxidation mixture of 1 for 3 h (blue solid line) in THF.

Such remarkable reactivity of the opda moiety in 1·THF toward air oxidation cannot be obtained for noncoordinating opda, indicating the essential role of the Fe(II) ion. This Fe(II)-assisted ligand-centered air oxidation activity for 1 guarantees the $2\text{H}^+/2\text{e}^-$ pooling ability of Fe(II)-bound opda.

During the air oxidation of 1, stepwise color changes were obtained (see Supporting Information). It is noteworthy that the reaction mixture after the HER shows characteristic absorptions at 420 and 720 nm (Figure 6, green dashed line), unlike those of 1, with absorption maxima near to those observed during air oxidation of 1 (Figure 6, blue solid line). Moreover, in the ESI-MS spectrum of the HER mixture from

3opda/ Fe^{II} /THF in CH_3CN , several peaks, i.e., $[\text{Fe}^{\text{II}}(\text{bqdi})_2]-(\text{C}_6\text{H}_4\text{N}_2\text{H}_3)^+$ ($m/z = 373.09$), $[\text{Fe}^{\text{II}}(\text{bqdi})(\text{opda})_2]-(\text{CH}_3\text{CN})_2^{2+}-\text{H}^+$ ($m/z = 459.36$), assignable to fragments containing the bqdi moiety were obtained (Figure 7d). On the

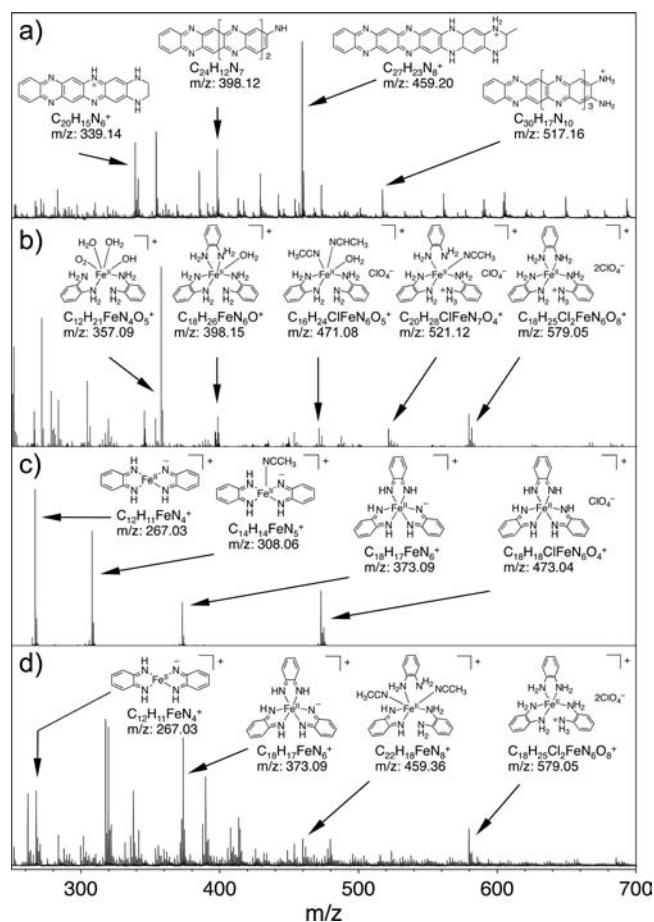


Figure 7. ESI-MS spectra of (a) HER reaction mixture from 3opda/THF solution, (b) 1, (c) 2, and (d) HER reaction mixture from 3opda/ $[\text{Fe}^{\text{II}}(\text{H}_2\text{O})_6](\text{ClO}_4)_2$ /THF suspension (CH_3CN , m/z 250–700, positive ion mode).

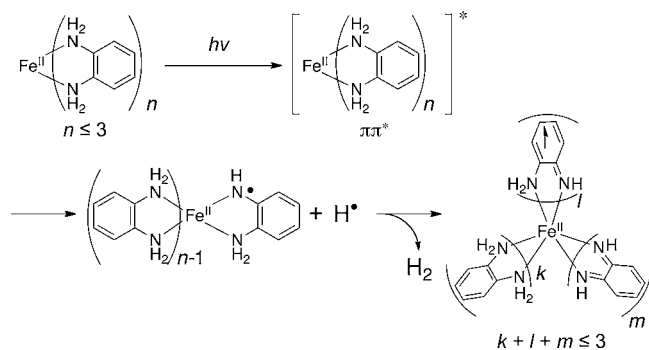
basis of these results, similar to the case of air oxidation of 1, oxidation of the opda moiety in 1 generating s-bqdi or bqdi can be considered also in the HER. The residual opda in the MS spectrum indicates the incompleteness of the HER. The reason is not clear at this stage, but plausibly the side product could inhibit the HER. In addition, fragment peaks implying oligomeric species of opda were obtained in the MS spectrum of the HER mixture from 3opda/THF. They indicate the existence of bqdi as transient species, which are known to produce 2,3-diaminophenazine derivatives through [2 + 4] cycloaddition processes with unreacted opda.³⁶ These oligomeric species are not obtained in the HER mixture from 3opda/ Fe^{II} /THF, suggesting that photochemically generated bqdi should be stabilized by coordination to the coexisting Fe^{II} center by σ -donation and π -back-donation,³⁷ thereby [2 + 4] cycloaddition with unreacted opda should be inhibited.

Reaction Mechanism of HER. In previous reports on the photochemistry of aromatic amines or diamines, it was shown that photochemical N–H σ -bond activation generates a transient anilino radical ($\text{C}_6\text{H}_5\text{NH}\cdot$), semibenzoquinodiimine, or benzoquinodiimine via hydrogen atom elimination initiated

by photoexcitation of a $\pi\pi^*$ transition through the 3s Rydberg state of the nitrogen atoms ($1\pi\sigma^*$), using several spectroscopic and theoretical techniques.^{20,21} Based on these well-established studies, it is presumed that the HER from the 3opda/Fe(II)/THF mixture would proceed through a $\pi\pi^*$ transition followed by N–H dissociation in the opda moiety to produce bqdi or s-bqdi that is plausibly coordinating to Fe ion. In the TD-DFT calculation for opda, it was shown that the $1\pi\sigma^*$ state lies slightly above the $1\pi\pi^*$ state (see Supporting Information for details), which supports this presumption. The higher HER efficiency from the 3opda/Fe(II)/THF sample, than from the 3opda/THF solution, indicates the essential role of the Fe(II) ion in promoting HER. As one of the possibilities, an assembling effect of opda moieties could be considered by coordination to the cationic Fe(II) center throughout the reaction, which would let the photochemically generated hydrogen atom react with the other NH₂ groups coordinating the Fe(II) center.

From a consideration of these results, a plausible mechanism for the HER of **1** could be described as follows: (1) $\pi\pi^*$ excited state formed by irradiation at around 298 nm; (2) N–H σ -bond elimination to produce hydrogen atom and Fe(II) complex of *o*-aminoanilino radical, equivalent to the s-bqdi, species; and (3) hydrogen atom abstraction from s-bqdi or unreacted opda to produce a H₂ molecule and partially oxidized species of the Fe(II) complex, probably such as $[\text{Fe}^{\text{II}}(\text{opda})_k(\text{s-bqdi})_l(\text{bqdi})_m]^{2+}$ ($k + l + m \leq 3$) (Scheme 1).

Scheme 1. Plausible Mechanism for Photochemical HER from the 3opda/[Fe^{II}(H₂O)₆](ClO₄)₂/THF Mixture



Photocatalytic HER Using HQ as a H⁺/e⁻ Donor. For the creation of photocatalytic HER systems, the HER from a mixture of opda and $[\text{Fe}^{\text{II}}(\text{H}_2\text{O})_6](\text{ClO}_4)_2$ in the presence of HQ as an additional H⁺/e⁻ mediator was conducted (Figure 8, green circles). HQ derivatives are known to possess reversible 2H⁺/2e⁻ transfer capability, the same as for opda.³⁸ By the addition of 10 equiv of HQ to the opda and Fe(II) mixture, the amount of photochemically evolved hydrogen was continuously increased, even after 57 h, in contrast to the case without HQ (Figure 8, red circles). The amount of evolved hydrogen was 3.41×10^{-4} mol (TON = 4.28) after 196 h, which is about four times as much as that without HQ (8.77×10^{-5} mol after 57 h), suggesting that HQ serves as a H⁺/e⁻ donor for these reactions. In the cases of two control experiments without both opda and Fe(II) or opda under the same conditions (Figure 8, black and brown circles), the HER could not be obtained, suggesting the inertness of HQ itself for photochemical HER together with the catalytic role of the complex species

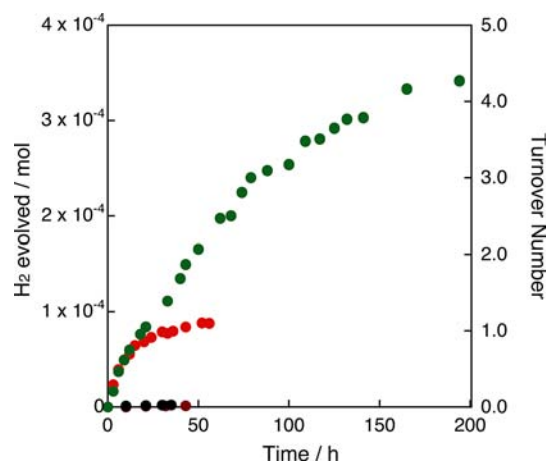


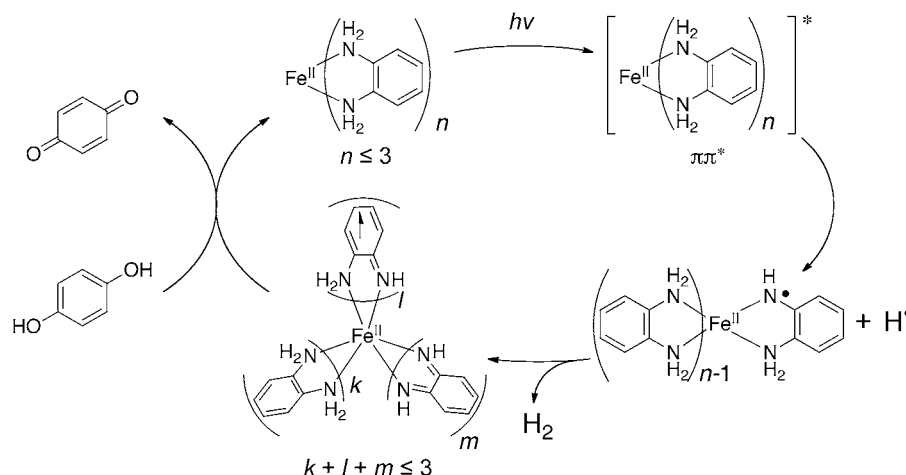
Figure 8. Amounts of photochemically produced hydrogen from 3opda/[Fe^{II}(H₂O)₆](ClO₄)₂/10HQ/THF (green circles), 3opda/[Fe^{II}(H₂O)₆](ClO₄)₂/THF (red circles) suspensions, 10HQ/THF (black circles), and [Fe^{II}(H₂O)₆](ClO₄)₂/10HQ/THF (brown circles) solutions.

consisting of opda(s) and Fe(II) or its partially oxidized species.

On the other hand, a similar photochemical HER using opda, $[\text{Fe}^{\text{II}}(\text{H}_2\text{O})_6](\text{ClO}_4)_2$, and HQ-*d*₂ (C₆H₄O₂D₂), in which the deuteration ratio on the hydroxyl groups was determined to be 85% by ¹H NMR, instead of HQ, D₂ and HD were obtained (Figure 3e and see Supporting Information). Although the possibilities not only that D⁺ of HQ-*d*₂ transferred in the photochemical HER mechanism but also that opda was deuterated by H/D exchange between HQ-*d*₂ before photoirradiation should be taken into account, it is suggested that the H⁺ of HQ can be the source of photochemically evolved H₂ in this HER. In the ¹H NMR spectrum of product after the catalytic HER in DMSO-*d*₆, the existence of *p*-benzoquinone (BQ) was indicated, supporting these considerations (see Supporting Information). From these comprehensive considerations, a plausible HER reaction cycle can be described as shown in Scheme 2. The HQ apparently serves as the proton/electron sacrifice reagent during the HER. Since the photoirradiation experiments for 2/10HQ/THF did not lead to detectable hydrogen, HQ might interact with partially oxidized species derived from **1** at either ground or excited states or both. Furthermore, HQ is an expected H⁺/e⁻ mediator in an extended system for hydrogen production based on this HER cycle.

CONCLUSION

In summary, this paper exploited a novel system toward the photochemical HER, where the opda combined with a nonprecious-metal ion, such as Fe^{II}, can effectively serve as H⁺/e⁻ poolers. A key feature is to make effective coordination interaction between metal ions with the opda moieties. Light irradiation onto the pooler initiates the HER, and successive H⁺ and e⁻ transfers proceed from HQ. The results presented here provide one possible way to activate organic moieties supported with nonprecious metals. Efforts are presently focused on deepening our understanding of the mechanism, as well as improvements in the catalytic activity, together with the tuning of HOMO–LUMO gaps to realize hydrogen production/storage operative with visible light.

Scheme 2. Plausible Mechanism for Photochemical HER from the 3opda/[Fe^{II}(H₂O)₆](ClO₄)₂/10HQ/THF Mixture

■ ASSOCIATED CONTENT

Supporting Information

GC analyses results of photochemical HER. Movie of photochemical HER from 3opda/Fe^{II}/THF suspension. Bond distances (Å) and dihedral angles (η) of 1·THF and 2·THF. IR spectra of 1·THF and white powder sample. Optimized structures and Cartesian coordinates for [Fe^{II}(opda)₃]²⁺, opda, and [Fe^{II}(bqdi)₃]²⁺. Molecular orbitals, simulated absorption spectra, and vertical excitation energies of [Fe^{II}(opda)₃]²⁺, opda, and [Fe^{II}(bqdi)₃]²⁺. UV-vis NIR absorption spectrum of 1 and relative light intensity of the light source (xenon lamp), transmission spectra of UVA-type mirror module, VIS-type mirror module, and band-pass filter (HQBP300-UV), and irradiation light dependence of the HER. Details of the apparent quantum yield calculation. These materials are available free of charge via the Internet at <http://pubs.acs.org>.

■ AUTHOR INFORMATION

Corresponding Author

chang@sci.hokudai.ac.jp; mkato@sci.hokudai.ac.jp

Notes

The authors declare no competing financial interest.

■ ACKNOWLEDGMENTS

The authors are grateful to emeritus Prof. Yoichi Sasaki, Prof. Kohei Uosaki, and Prof. Kei Murakoshi for discussions. The authors are grateful to Mr. Koichi Shiomi (Shimadzu Analytical & Measuring Center Inc.) for great support and discussions on D₂/HD/H₂ detection by GC. The authors are grateful to Prof. Noboru Kitamura (Hokkaido Univ.) and Prof. Eri Sakuda (Hokkaido Univ.) for their support on ESI-MS measurements. The authors are grateful to Prof. Takayoshi Nakamura (Hokkaido Univ.) and Prof. Shin-ichiro Noro (Hokkaido Univ.) for their support on magnetic measurements. This work was supported by the Elements Science and Technology Project “Nano-Hybridized Precious-Metal-Free Catalysts for Chemical Energy Conversion”, a Grant-in-Aid for Scientific Research for Priority Area “Coordination Programming” (area no. 2107), Creative Research Institution, Hokkaido University, Japan, Shorai Foundation for Science and Technology, JGC-S Scholarship Foundation, and a Grants-in-Aid for Scientific

Research (B) (23350025) from the Ministry of Education, Culture, Sports, Science, and Technology (MEXT), Japan.

■ REFERENCES

- (1) Armaroli, N.; Balzani, V. *Angew. Chem., Int. Ed.* **2007**, *46*, 52–66.
- (2) Kamat, P. V. *J. Phys. Chem. C* **2007**, *111*, 2834–2860.
- (3) Züttel, A.; Remhof, A.; Borgschulte, A.; Friedrichs, O. *Philos. Trans. R. Soc., A* **2010**, *368*, 3329–3342.
- (4) (a) Mazloomi, K.; Gomes, C. *Renewable Sustainable Energy Rev* **2012**, *16*, 3024–3033. (b) Lewis, N. S.; Nocera, D. G. *Proc. Natl. Acad. Sci. U.S.A.* **2006**, *103*, 15729–15735.
- (5) (a) Suh, M. P.; Park, H. J.; Prasad, T. K.; Lim, D.-W. *Chem. Rev.* **2011**, *112*, 782–835. (b) Eberle, U.; Felderhoff, M.; Schüth, F. *Angew. Chem., Int. Ed.* **2009**, *48*, 6608–6630.
- (6) Sakintuna, B.; Lamari-Darkrim, F.; Hirscher, M. *Int. J. Hydrogen Energy* **2007**, *32*, 1121–1140.
- (7) (a) Schuth, F.; Bogdanovic, B.; Felderhoff, M. *Chem. Commun.* **2004**, 2249–2258. (b) Orimo, S.-i.; Nakamori, Y.; Eliseo, J. R.; Züttel, A.; Jensen, C. M. *Chem. Rev.* **2007**, *107*, 4111–4132. (c) Grochala, W.; Edwards, P. P. *Chem. Rev.* **2004**, *104*, 1283–1316. (d) Christensen, C. H.; Sorensen, R. Z.; Johannessen, T.; Quaaade, U. J.; Honkala, K.; Elmoe, T. D.; Kohler, R.; Norskov, J. K. *J. Mater. Chem.* **2005**, *15*, 4106–4108.
- (8) (a) Hügle, T.; Hartl, M.; Lentz, D. *Chem.—Eur. J.* **2011**, *17*, 10184–10207. (b) Alcaraz, G.; Sabo-Etienne, S. *Angew. Chem., Int. Ed.* **2010**, *49*, 7170–7179. (c) Hamilton, C. W.; Baker, R. T.; Staubitz, A.; Manners, I. *Chem. Soc. Rev.* **2009**, *38*, 279–293.
- (9) Struzhkin, V. V.; Militzer, B.; Mao, W. L.; Mao, H.-k.; Hemley, R. J. *Chem. Rev.* **2007**, *107*, 4133–4151.
- (10) Chen, J.; Wu, F. *Appl. Phys. A: Mater. Sci. Process.* **2004**, *78*, 989–994.
- (11) (a) Cheng, H.-M.; Yang, Q.-H.; Liu, C. *Carbon* **2001**, *39*, 1447–1454. (b) Baughman, R. H.; Zakhidov, A. A.; de Heer, W. A. *Science* **2002**, *297*, 787–792. (c) Ströbel, R.; Garche, J.; Moseley, P. T.; Jörissen, L.; Wolf, G. *J. Power Sources* **2006**, *159*, 781–801.
- (12) Kubota, Y.; Takata, M.; Matsuda, R.; Kitaura, R.; Kitagawa, S.; Kato, K.; Sakata, M.; Kobayashi, T. C. *Angew. Chem., Int. Ed.* **2005**, *44*, 920–923.
- (13) (a) Dobereiner, G. E.; Nova, A.; Schley, N. D.; Hazari, N.; Miller, S. J.; Eisenstein, O.; Crabtree, R. H. *J. Am. Chem. Soc.* **2011**, *133*, 7547–7562. (b) Yamaguchi, R.; Ikeda, C.; Takahashi, Y.; Fujita, K.-i. *J. Am. Chem. Soc.* **2009**, *131*, 8410–8412. (c) Jessop, P. *Nat. Chem.* **2009**, *1*, 350–351.
- (14) (a) Kawahara, R.; Fujita, K.-i.; Yamaguchi, R. *Angew. Chem.* **2012**, *124*, 12962–12966. (b) Kawahara, R.; Fujita, K.-i.; Yamaguchi, R. *J. Am. Chem. Soc.* **2012**, *134*, 3643–3646.
- (15) (a) Tinker, L. L.; McDaniel, N. D.; Curtin, P. N.; Smith, C. K.; Ireland, M. J.; Bernhard, S. *Chem.—Eur. J.* **2007**, *13*, 8726–8732.

- (b) Elvington, M.; Brown, J.; Arachchige, S. M.; Brewer, K. J. *J. Am. Chem. Soc.* **2007**, *129*, 10644–10645. (c) Goldsmith, J. L.; Hudson, W. R.; Lowry, M. S.; Anderson, T. H.; Bernhard, S. *J. Am. Chem. Soc.* **2005**, *127*, 7502–7510. (d) Esswein, A. J.; Nocera, D. G. *Chem. Rev.* **2007**, *107*, 4022–4047. (e) Ozawa, H.; Sakai, K. *Chem. Commun.* **2011**, *47*, 2227–2242. (f) Sakai, K.; Ozawa, H. *Coord. Chem. Rev.* **2007**, *251*, 2753–2766. (g) Inagaki, A.; Akita, M. *Coord. Chem. Rev.* **2010**, *254*, 1220–1239. (h) Wang, M.; Na, Y.; Gorlov, M.; Sun, L. *Dalton Trans.* **2009**, 6458–6467. (i) Fukuzumi, S.; Suenobu, T. *Dalton Trans.* **2013**, *42*, 18–28. (j) Hull, J. F.; Himeda, Y.; Wang, W.-H.; Hashiguchi, B.; Periana, R.; Szalda, D. J.; Muckerman, J. T.; Fujita, E. *Nat. Chem.* **2012**, *4*, 383–388. (k) Maeda, K.; Higashi, M.; Lu, D.; Abe, R.; Domen, K. *J. Am. Chem. Soc.* **2010**, *132*, 5858–5868.
- (16) (a) McNamara, W. R.; Han, Z.; Alperin, P. J.; Brennessel, W. W.; Holland, P. L.; Eisenberg, R. *J. Am. Chem. Soc.* **2011**, *133*, 15368–15371. (b) Lazarides, T.; McCormick, T.; Du, P.; Luo, G.; Lindley, B.; Eisenberg, R. *J. Am. Chem. Soc.* **2009**, *131*, 9192–9194. (c) Kaur-Ghumaan, S.; Schwartz, L.; Lomoth, R.; Stein, M.; Ott, S. *Angew. Chem., Int. Ed.* **2010**, *49*, 8033–8036. (d) McCormick, T. M.; Han, Z.; Weinberg, D. J.; Brennessel, W. W.; Holland, P. L.; Eisenberg, R. *Inorg. Chem.* **2011**, *50*, 10660–10666. (e) Lee, C. H.; Dogutan, D. K.; Nocera, D. G. *J. Am. Chem. Soc.* **2011**, *133*, 8775–8777. (f) Sun, Y.; Bigi, J. P.; Piro, N. A.; Tang, M. L.; Long, J. R.; Chang, C. J. *J. Am. Chem. Soc.* **2011**, *133*, 9212–9215. (g) Zhang, W.; Hong, J.; Zheng, J.; Huang, Z.; Zhou, J.; Xu, R. *J. Am. Chem. Soc.* **2011**, *133*, 20680–20683. (h) Streich, D.; Astuti, Y.; Orlandi, M.; Schwartz, L.; Lomoth, R.; Hammarström, L.; Ott, S. *Chem.—Eur. J.* **2010**, *16*, 60–63. (i) Karunadasa, H. I.; Chang, C. J.; Long, J. R. *Nature* **2010**, *464*, 1329–1333. (j) Rakowski Dubois, M.; Dubois, D. L. *Acc. Chem. Res.* **2009**, *42*, 1974–1982. (k) Artero, V.; Chavarot-Kerlidou, M.; Fontecave, M. *Angew. Chem., Int. Ed.* **2011**, *50*, 7238–7266. (l) Dempsey, J. L.; Brunschwig, B. S.; Winkler, J. R.; Gray, H. B. *Acc. Chem. Res.* **2009**, *42*, 1995–2004. (m) Cook, T. R.; Dogutan, D. K.; Reece, S. Y.; Surendranath, Y.; Teets, T. S.; Nocera, D. G. *Chem. Rev.* **2010**, *110*, 6474–6502. (n) Walter, M. G.; Warren, E. L.; McKone, J. R.; Boettcher, S. W.; Mi, Q.; Santori, E. A.; Lewis, N. S. *Chem. Rev.* **2010**, *110*, 6446–6473. (o) Losse, S.; Vos, J. G.; Rau, S. *Coord. Chem. Rev.* **2010**, *254*, 2492–2504.
- (17) (a) Cui, R.; Huang, H.; Yin, Z.; Gao, D.; Zhu, J.-J. *Biosens. Bioelectron.* **2008**, *23*, 1666–1673. (b) Muñoz-Muñoz, J. L.; Garcia-Molina, F.; Berna, J.; Garcia-Ruiz, P. A.; Varon, R.; Tudela, J.; Rodriguez-Lopez, J. N.; Garcia-Canovas, F. *Biochim. Biophys. Acta, Proteins Proteomics* **2012**, *1824*, 647–655. (c) Peng, J.; Feng, L.-N.; Zhang, K.; Li, X.-H.; Jiang, L.-P.; Zhu, J.-J. *Chem.—Eur. J.* **2012**, *18*, 5261–5268.
- (18) (a) Song, N.; Gagliardi, C. J.; Binstead, R. A.; Zhang, M.-T.; Thorp, H.; Meyer, T. J. *J. Am. Chem. Soc.* **2012**, *134*, 18538–18541. (b) Walczak, M. M.; Dryer, D. A.; Jacobson, D. D.; Foss, M. G.; Flynn, N. T. *J. Chem. Educ.* **1997**, *74*, 1195.
- (19) (a) Warren, L. F. *Inorg. Chem.* **1977**, *16*, 2814–2819. (b) Peng, S. M.; Chen, C. T.; Liaw, D. S.; Chen, C. L.; Wang, Y. *Inorg. Chim. Acta* **1985**, *101*, L31–L33. (c) Konno, Y.; Matsushita, N. *Bull. Chem. Soc. Jpn.* **2006**, *79*, 1046–1053. (d) Bugarcic, T.; Habtemariam, A.; Deeth, R. J.; Fabbiani, F. P. A.; Parsons, S.; Sadler, P. J. *Inorg. Chem.* **2009**, *48*, 9444–9453. (e) Kapovsky, M.; Dares, C.; Dodsworth, E. S.; Begum, R. A.; Raco, V.; Lever, A. B. P. *Inorg. Chem.* **2012**, *52*, 169–181.
- (20) (a) Roberts, G. M.; Williams, C. A.; Young, J. D.; Ullrich, S.; Paterson, M. J.; Stavros, V. G. *J. Am. Chem. Soc.* **2012**, *134*, 12578–12589. (b) Montero, R.; Conde, A. P.; Ovejas, V.; Martinez, R.; Castano, F.; Longarte, A. *J. Chem. Phys.* **2011**, *135*, 054308–054308. (c) King, G. A.; Oliver, T. A. A.; Ashfold, M. N. R. *J. Chem. Phys.* **2010**, *132*, 214307–214312.
- (21) (a) Ujike, K.; Akai, N.; Kudoh, S.; Nakata, M. *J. Mol. Struct.* **2005**, *735–736*, 335–342. (b) Ujike, K.; Kudoh, S.; Nakata, M. *Chem. Phys. Lett.* **2004**, *396*, 288–292.
- (22) Cossi, M.; Scalmani, G.; Rega, N.; Barone, V. *J. Chem. Phys.* **2002**, *117*, 43–54.
- (23) Rappe, A. K.; Casewit, C. J.; Colwell, K. S.; Goddard, W. A.; Skiff, W. M. *J. Am. Chem. Soc.* **1992**, *114*, 10024–10035.
- (24) (a) Bauernschmitt, R. d.; Ahlrichs, R. *Chem. Phys. Lett.* **1996**, *256*, 454–464. (b) Dreuw, A.; Head-Gordon, M. *Chem. Rev.* **2005**, *105*, 4009–4037.
- (25) Iikura, H.; Tsuneda, T.; Yanai, T.; Hirao, K. *J. Chem. Phys.* **2001**, *115*, 3540–3544.
- (26) Frisch, M. J.; Trucks, G. W.; Schlegel, H. B.; Scuseria, G. E.; Robb, M. A.; Cheeseman, J. R.; Scalmani, G.; Barone, V.; Mennucci, B.; Petersson, G. A.; Nakatsuji, H.; Caricato, M.; Li, X.; Hratchian, H. P.; Izmaylov, A. F.; Bloino, J.; Zheng, G.; Sonnenberg, J. L.; Hada, M.; Ehara, M.; Toyota, K.; Fukuda, R.; Hasegawa, J.; Ishida, M.; Nakajima, T.; Honda, Y.; Kitao, O.; Nakai, H.; Vreven, T.; Montgomery, J. A.; Peralta, J. E.; Ogliaro, F.; Bearpark, M.; Heyd, J. J.; Brothers, E.; Kudin, K. N.; Staroverov, V. N.; Kobayashi, R.; Normand, J.; Raghavachari, K.; Rendell, A.; Burant, J. C.; Iyengar, S. S.; Tomasi, J.; Cossi, M.; Rega, N.; Millam, J. M.; Klene, M.; Knox, J. E.; Cross, J. B.; Bakken, V.; Adamo, C.; Jaramillo, J.; Gomperts, R.; Stratmann, R. E.; Yazyev, O.; Austin, A. J.; Cammi, R.; Pomelli, C.; Ochterski, J. W.; Martin, R. L.; Morokuma, K.; Zakrzewski, V. G.; Voth, G. A.; Salvador, P.; Dannenberg, J. J.; Dapprich, S.; Daniels, A. D.; Farkas, Foresman, J. B.; Ortiz, J. V.; Cioslowski, J.; Fox, D. J. *Gaussian 09*, revision A.02; Gaussian, Inc.: Wallingford, CT, 2009.
- (27) Martin, R. L. *J. Chem. Phys.* **2003**, *118*, 4775–4777.
- (28) Kahn, O. *Molecular Magnetism*; Wiley-VCH: New York, 1993; p 380.
- (29) Fulmer, G. R.; Miller, A. J. M.; Sherden, N. H.; Gottlieb, H. E.; Nudelman, A.; Stoltz, B. M.; Bercaw, J. E.; Goldberg, K. I. *Organometallics* **2010**, *29*, 2176–2179.
- (30) Burla, M. C.; Caliendo, R.; Camalli, M.; Carrozzini, B.; Cascarano, G. L.; De Caro, L.; Giacovazzo, C.; Polidori, G.; Spagna, R. *J. Appl. Crystallogr.* **2005**, *38*, 381–388.
- (31) *CrystalStructure 3.8.2, Crystal Structure Analysis Package*; Rigaku and Rigaku/MS: The Woodlands, TX, 2000–2006.
- (32) Sheldrick, G. *SHELX-97 Program for Crystal Structure Solution and the Refinement of Crystal Structures*; Institut für Anorganische Chemie der Universität Göttingen: Göttingen, Germany, 1997.
- (33) Czapik, A.; Gdaniec, M. *Acta Crystallogr. Sect. C: Cryst. Struct. Commun.* **2010**, *C66*, o198–o201.
- (34) (a) Bing, Y.; Qiuye, L.; Hideo, I.; Tetsuya, K.; Jinhua, Y. *Sci. Technol. Adv. Mater.* **2011**, *12*, 034401. (b) Wang, D.; Kako, T.; Ye, J. *J. Phys. Chem. C* **2009**, *113*, 3785–3792. (c) Chen, D.; Ye, J. *Chem. Mater.* **2009**, *21*, 2327–2333.
- (35) (a) Milliken, B.; Borer, L.; Russell, J.; Bilich, M.; Olmstead, M. M. *Inorg. Chim. Acta* **2003**, *348*, 212–216. (b) Cheng, H. Y.; Peng, S. M. *Inorg. Chim. Acta* **1990**, *169*, 23–24.
- (36) Loveless, N. P.; Brown, K. C.; Horrocks, R. H. *J. Org. Chem.* **1981**, *46*, 1182–1185.
- (37) Gorelsky, S. I.; Dodsworth, E. S.; Lever, A. B. P.; Vlcek, A. A. *Coord. Chem. Rev.* **1998**, *174*, 469–494.
- (38) Piera, J.; Bäckvall, J.-E. *Angew. Chem., Int. Ed.* **2008**, *47*, 3506–3523.